Experimental study on the two-phase pressure drop in copper foams

Xianbing Ji & Jinliang Xu

Heat and Mass Transfer
Wärme- und Stoffübertragung

ISSN 0947-7411
Volume 48
Number 1

Heat Mass Transfer (2012) 48:153-164
DOI 10.1007/s00231-011-0860-2

Springer

Heat Mass Transfer (2012) 48:153–164
DOI 10.1007/s00231-011-0860-2

ORIGINAL

Experimental study on the two-phase pressure drop in copper foams

Xianbing Ji · Jinliang Xu

Received: 3 April 2011 / Accepted: 30 June 2011 / Published online: 15 July 2011

Abstract Experiments were performed to study pressure drops in copper foams embedded in a rectangular copper channel. De-ionized water was used as the working fluid with mass fluxes of 30–200 kg/m^2 s, and inlet temperature of 40–80°C. The copper foam has the porosity of 0.88 and the pore densities of 30, 60 and 90 ppi (pores per inch). Both single-phase liquid flow and boiling two-phase flow are studied. Effects of mass fluxes, vapor mass qualities, and average pore diameters of metallic foams are investigated. It is found that friction factors for the single-phase liquid flow are mainly dependent on the Reynolds number and the average pore diameter of metallic foams. The friction factors are decreased with increases in the Reynolds numbers, and will approach 0.22 at high Reynolds numbers. For the boiling two-phase flow, two-phase pressure drops are increased with increases in the outlet vapor mass qualities, mass fluxes, and ppi values. The two-phase multiplier is increased with increases in the outlet vapor mass qualities and mass fluxes, and it is decreased with increases in the Martinelli parameter and will attain a constant value depending on the mass fluxes. The larger the mass fluxes, the larger the constant value is. An experimental correlation considering the effects of vapor mass qualities, mass fluxes, and average pore diameters of metallic foams is recommended, showing good accuracy to predict the two-phase pressure drops in metallic foams.

Keywords Metallic foam · Flow boiling · Pressure drop

X. Ji · J. Xu
State Key Laboratory of Alternate Electrical Power System with Renewable Energy Sources, North China Electric Power University, Beijing 102206, People's Republic of China

J. Xu (✉)
The Beijing Key Laboratory of New and Renewable Energy, North China Electric Power University, Beijing 102206, People's Republic of China
e-mail: xjl@ncepu.edu.cn

List of symbols

C	Constant coefficient
C_o	Form coefficient of channel
C_{pl}	Specific heat of liquid (J/kgK)
D_p	Equivalent diameter of metallic foams (m)
d_{f}	Ligament diameter of metallic foam (m)
d_{p}	Pore diameter of metallic foam (m)
d_h	Hydraulic diameter of the channel (m)
d_m	Average pore diameter of metallic foam (m)
G	Mass flux (kg/m^{2}s)
f_k	Friction factor for the single-phase liquid flow in metallic foams
H	Height of the rectangular channel (m)
h_{lg}	Latent heat of evaporation (J/kg)
I	Electric current (A)
K	Permeability (m$^{2)}$
L	Channel length (m)
l	Ligament length of a unit cell of metallic foams (m)
m	Mass flow rate (kg/s)
p	Pressure (Pa)
ppi	number of pores per inch for the metallic foam
q	Heat flux (W/m^2)
Q	Effective heating power (J)
Re_p	Reynolds number based on porous media
S_c	Cross-sectional area of channel (m^2)
S_v	Solid surface area per unit volume (1/m)
T	Temperature (K or °C)
t	Time (s)

U Voltage (V)
u Velocity (m/s)
X_{vv} Martinelli parameter
x Thermodynamic vapor mass quality
W Channel width (m)
z Axial flow coordinate (m)
$\frac{dp}{dz}$ Pressure gradient along the flow direction (Pa/m)
Δp Pressure drop (Pa)
Δp_c Pressure drop due to channel expansion or contraction (Pa)
Δp_a Acceleration pressure drop (Pa)
$\Delta p_{tp,f}$ Two-phase friction pressure drop (Pa)
α_{out} Void fraction at the channel outlet
ε Porosity of metallic foam
v Specific volume (m^3/kg)
μ Viscosity (kg/m s)
ρ Density (kg/m^3)
φ The ratio of heat received by the fluid to the applied heating power
ϕ_f^2 Two-phase friction multiplier based on liquid flow rate

Subscripts

l Liquid phase
g Vapor phase
sat Saturation condition
sp Single-phase
tp Two-phase
w Wall surface condition
in Inlet condition
out Outlet condition
pre Prediction
exp Experiment

1 Introduction

Flow and heat transfer characteristics in porous media have been studied widely in the past century. The early study can be tracked back to the Darcy law published in 1856 [1], which describes the relationship of pressure drop versus flow velocity and permeability. Following then other investigators modified the Darcy equation [2–4]. However, most of these studies refer to the porous media with low porosities, coving the range of 0.3–0.6. Examples are filled beds and particle media. Metallic foam was invented in the twentieth century, having advantageous of high porosity (can be larger than 0.8), ultra-light, uniform pore size, and high thermal conductivity of metallic ligament. Great attention has been paid on the flow and heat transfer in metallic foams.

Anothe et al. [5] and Lage et al. [6] investigated the flow characteristics with air flowing in various aluminum foams with different compressibility ratios. They found that the pressure gradient is increased with increases in the flow velocity. The pressure drop is found to have cubic relationship with flow velocity. Bastawros et al. [7, 8] obtained the power law relationship between the pressure drop and the flow velocity in the transition flow region ($Re_k = 1.01$), with the pore density of 30 ppi and porosity of 91.5%. The foam configuration parameters have significant effect on the pressure drops.

Kim et al. [9] investigated the friction pressure drop with water flowing in metallic foam fins. The foam porosity of the fin is 89–96%. It is shown that the friction pressure drop is influenced by the permeability and porosity. Crosnier et al. [10] studied the flow behavior in metallic foams with pore densities of 20, 40 and 60 ppi. The foam porosity is greater than 90%. Khayargoli et al. [11] investigated the micro structure effect on the flow characteristics in nickel and nickel–chromium foams. It is found that the pressure drop is decreased with increases in pore diameters and permeability, and with decreases in pore densities and form coefficients. It is noted that porosities have weak influences on the pressure drops.

Metallic foams are often used in compact heat exchangers. Dukhan et al. [12] measured and analyzed the flow behavior with air flowing in compressed and un-compressed metallic foams. They found that the pressure drop is obviously increased when compressed metallic foams are used. Compared with the results reported previously, the foam permeability is well predicted, but the inertia coefficient is not well handled.

Medraj et al. [13] investigated the permeability of air flowing in simple and complex metallic foams. For simple-structured metallic foams, the effect of pore diameter on the permeability is similar to those reported by other investigators. For complex-structured metallic foams, the permeability is decreased with increases in pore diameters. However, no matter for simple or complex-structured metallic foams, the pressure drop is decreased with increases in porosities, which is consistent with other studies in the literature. Recently, Salas and Waas [14] studied the effect of the foam thickness on the flow and heat transfer in metallic foams. The boiling two-phase pressure drop in metallic foams is less reported in the references. Bonnet et al. [15] performed experiments for co-current flow of a water–air mixture using 5 mm–2 cm thick foam samples. They analyzed different flow patterns and used the homogeneous model, Lockart–Martinelli model and separated flow model to calculate two-phase pressure drops in foams. Gerbaux et al. [16] performed experiments to determine the hydraulic parameters and characterize single-phase air flow and two-phase air–water flow in thin metallic foams with thickness of 1.5 mm. Three types of nickel foams are investigated. In the flow

rate range tested, their results along with former studies indicate the importance of the inertial effects. Zhao et al. [17] experimentally studied the boiling heat transfer in horizontal metal-foam filled tubes, showing that pressure drops are nonlinearly increased with the vapor mass qualities and mass flow rates. The metal-foam cell size has a significant effect on the pressure drop, which is doubled by reducing the foam cell size from 20 to 40 ppi. The pressure drop can be reduced by increasing operating pressures.

The objective of this study is to investigate pressure drops in a rectangular channel soldered with copper foams. The rectangular channel has the dimensions of 52.0 × 8.0 × 3.0 mm. The channel size used in this study is comparable to that of electronic chips with larger length to width ratio. The copper foam has the porosity of 0.88 and the pore densities of 30, 60 and 90 ppi. Both the single-phase liquid flow and the boiling two-phase flow are studied. Effects of the mass fluxes, vapor mass qualities, and average pore diameters of the metallic foams are studied. New correlations for both single-phase liquid flow and boiling flow are recommended. The present study is useful for the compact heat exchanger design using metallic foams.

2 Experimental facilities and setup

Figure 1 shows the experimental setup, consisting of subsystems of liquid supply, heating, rectangular channel test section soldered with copper foams, cooling, and data acquisition. A pump drives the liquid (de-ionized and de-gassed water in this study) to the test section. A bypass line is used to adjust the flow rate to the test section. A filter before the test section prevents solid particles entering the test section. The flow rate is measured by an orifice flow meter. In order to fit a wide flow rate range, three exchangeable orifices are used, with the orifice diameters of 2.0, 1.4, and 1.0 mm, respectively. The maximum flow rate can reach 48 kg/h. A constant temperature bath was arranged before the liquid enters the test section, keeping a constant liquid temperature at the channel inlet. The pressure drop is measured by a Senex pressure drop transducer across the tests section. A pressure transducer is also installed at the inlet of the test section. Two K-type thermocouples measured the fluid temperatures, arranged at the inlet and outlet of the test section. All the signals were recorded by a high speed data acquisition system. The power supplied to the channel test section was provided by cartridge heaters. Water was used as the working fluid, the physical properties are available in the open literature.

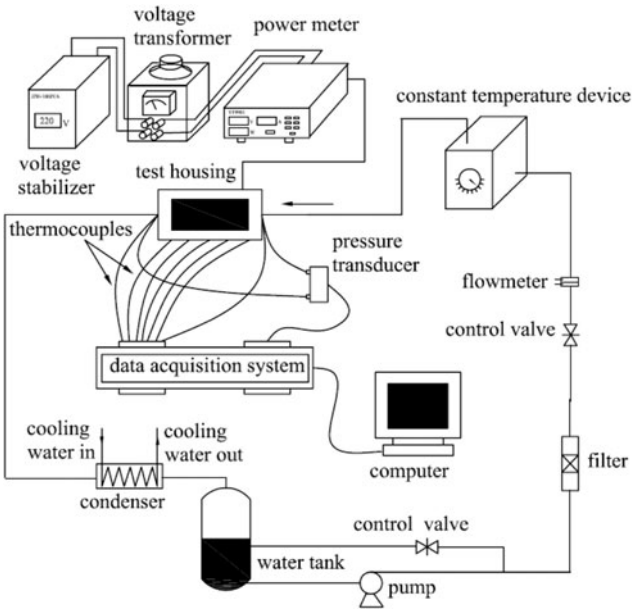

Fig. 1 The forced convection loop for the present experiment

Figure 2 shows the channel test section (not including the copper foam inserts). It consists of a copper body, cartridge heaters, and a Pyrex glass cover. The rectangular channel has a length of 52 mm, a width of 8.0 mm and a depth of 3.0 mm, respectively. The filled copper foam has exactly the same size as that of the rectangular channel. The copper foam is soldered with the rectangular channel surfaces. Thus the contact heat resistance between the copper foam and the channel surface can be neglected. The bottom heating section is divided into five separated parts, each consisting of two 100 W cartridge heaters with a diameter of 6.0 mm. Thus totally there are 10 cartridge heaters. The gap distance between two neighboring part is only 0.5 mm.

3 The copper foam and its characterization parameters

Figure 3 shows the three kinds of copper foams used in this study. The porosity is 0.88 and the pore densities are 30, 60 and 90 ppi, respectively. The foam has an open-celled structure composed of dodecahedron-like cells, having 12–14 pentagonal faces. It displays the three-dimensional web structure, forming numerous connected cells with metallic ligaments. The ligament length is l and diameter is d_f. The circumcircle diameter of the foam cell can be regarded as the pore diameter d_p. We measured the foam parameters by a Leica microscope. Table 1 shows the measured parameters. It is seen from Table 1 that the pore diameter, ligament length and diameter are decreased with increases in ppi values. In order to perform the calculations, various models of the foam structure are presented, such as the octahedron structure by Gibson and Ashy [18], hexahedron structure by Venkataranma and Sankar [19],

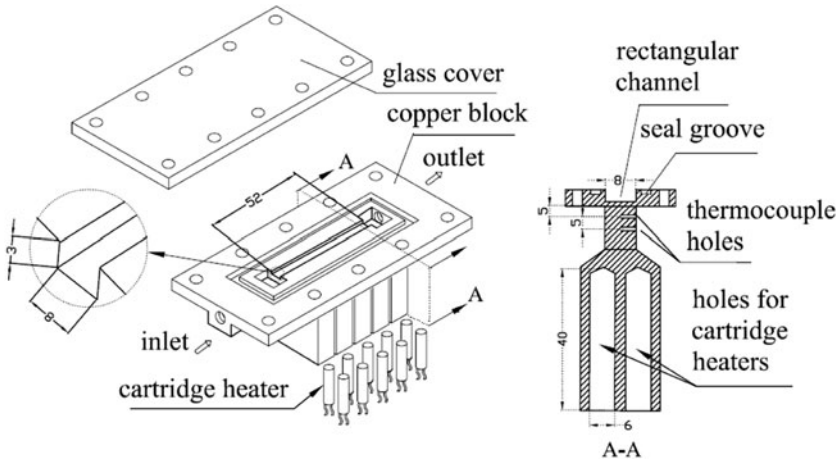

Fig. 2 The rectangular channel test section (copper foam not shown, the unit is mm)

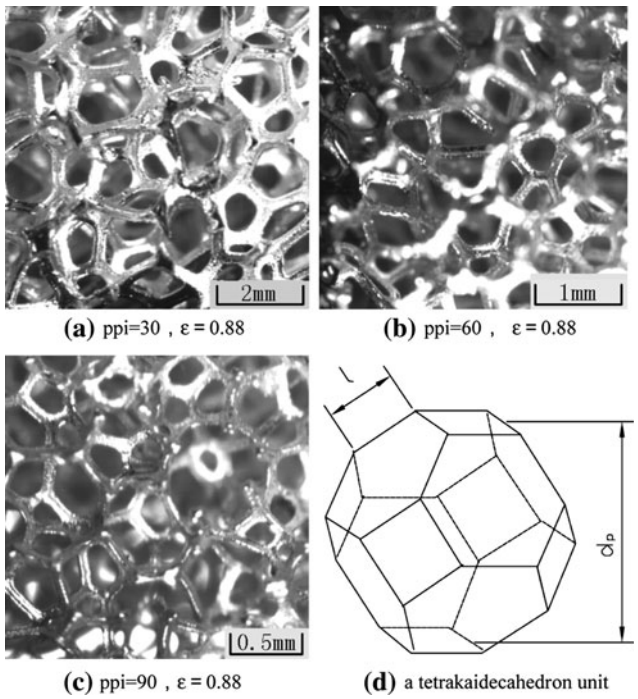

Fig. 3 The photos of copper foams (**a**, **b**, and **c**) and a unit foam cell represented by a tetrakaidecahedron unit (**d**)

and the widely accepted tetrakaidecahedron structure by Lord Kelvin [20]. The latest one may be reached as an ideal structure during the foam manufacturing process. The tetrakaidecahedron structure is helpful for the evaluation of the thermal conductivities of metallic foams (Table 2).

4 Data measurement and reduction

The measured parameters are summarized as follows:

Temperatures: The inlet/outlet fluid temperatures and wall temperatures are measured using k-type thermocouples with the response time of 0.2 s and uncertainties of 0.5°C.

Pressure and pressure drop: Pressure is measured at the inlet of the copper foam test section. Pressure drop is measured using a Senex pressure drop transducer, with a response time of 0.1 s and an uncertainty of 0.1%.

Mass flow rate: Mass flow rate is measured by an orifice flow meter. The pressure drop across the orifice flow meter is measured by a Senex pressure drop transducer. Calibration was performed for the output DC (direct current) voltage of the pressure drop transducer versus the mass flow rate.

Because the non-condensable gas has important effect on the boiling heat transfer in metallic foams, water (the working fluid in this study) is de-gassed by boiling the liquid for 2 h before the formal experiment to remove the non-condensable gas. The effective heat Q is defined as the net heat received by the fluid and calculated as $Q = \varphi UI$, where φ is the thermal efficiency, U is the voltage applied on the cartridge heaters and I is the current flowing through the cartridge heaters. A set of single-phase liquid flow and heat transfer experiments were performed to determine the thermal efficiency, most of data indicates that the thermal efficiency of 0.92 is suitable for the present experiment design.

Table 1 Thermophysical properties of water and vapor at atmospheric pressure (saturation condition)

T_{sat} (°C)	ρ_l (kg/m^3)	ρ_g (kg/m^3)	C_{pl} (kJ/kgK)	C_{pg} (kJ/kgK)	h_{lg} (kJ/kg)	σ (N/m)	μ_l Pa s	μ_g Pa s	k_f (W/mK)
100	958.4	0.597	4.22	2.03	2257	0.0589	0.000277	0.000012	0.683

Table 2 Parameters of the foam cells used in the present paper

ppi	ε	d_p (mm)	d_f (mm)	l (mm)	d_m (mm)	d_f/d_p
30	0.88	2.762	0.314	1.074	0.941	0.114
60	0.88	1.192	0.141	0.486	0.448	0.118
90	0.88	0.696	0.081	0.275	0.251	0.116

The heat flux was defined based on the three heating surfaces (two side walls and one bottom wall), q is written as

$$q = Q/(WL + 2HL) \tag{1}$$

where W, H, and L are the rectangular channel width, height, and length, respectively. The mean liquid flow velocity is written as

$$u = G/\rho_l = m/(\rho_l S_c) \tag{2}$$

where G is the mass flux, m is the mass flow rate, S_c is the cross sectional area of the channel.

During the experiment, subcooled liquid enters the test section. The pressure drop consists of two parts. One part corresponds to the single-phase liquid flow section (L_{sp}), the other corresponds to the boiling two-phase flow section (L_{tp}). The two sections are interfaced on the point where the thermodynamic vapor mass quality is zero (see Fig. 4).

The length of the single-phase liquid flow section is calculated as

$$L_{sp} = \frac{mC_{pl}L(T_{sat} - T_{in})}{Q} \tag{3}$$

where L is the total length of the rectangular channel, T_{sat} and T_{in} are the saturation temperature and inlet liquid temperature, respectively. The length of the two-phase flow section is $L_{tp} = L - L_{sp}$. The liquid temperature distribution along the flow direction in the single-phase liquid flow section is

$$T_l(z) = T_{in} + \frac{(T_{sat} - T_{in})z}{L_{sp}} \tag{4}$$

where z is the axial coordinate. The thermodynamic vapor mass quality is

$$x(z) = \frac{C_{pl}(T_{in} - T_{sat}) + zQ/mL}{h_{lg}} \tag{5}$$

where h_{lg} is the latent heat of evaporation.

5 Uncertainty analysis

The temperature measurements have an accuracy of 0.5°C. The heat flux has an uncertainty of 6%. The pressure and pressure drop measurements have accuracies of 0.1%. The mass flow rate and mass flux have uncertainties of 5.0 and 5.8%, respectively.

6 Results and discussion

6.1 The friction factor for the single-phase liquid flow

The friction factor for the single-phase liquid flow is necessary for the two-phase pressure drop calculation. For the flow in porous media, the pressure gradient can be calculated based on the Darcy equation in the laminar flow region.

$$\frac{dp}{dz} = \frac{\mu}{K}u \tag{6}$$

where μ is the fluid viscosity, K is the permeability. Equation 6 should be modified at high flow velocity, yielding the following Hazen-Dupuit-Darcy equation:

$$\frac{dp}{dz} = \frac{\mu}{K}u + \rho C_o u^2 \tag{7}$$

where C_o is the form coefficient of channel, which can be determined by the porosity and the channel dimensions

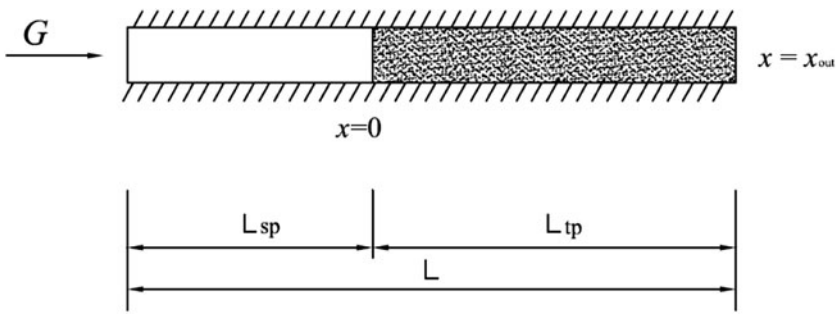

Fig. 4 A channel interfaced by single-phase flow section and two-phase flow section

filling the porous media [21]. Based on Eq. 7, different K and C_o are necessary to decide the pressure gradient for different metallic foams. The permeability K results in difficulties for the pressure gradient computation. Ergun [22] gave a pressure drop equation for the particle-based porous media:

$$\Delta p = \frac{f_k L \rho u^2 (1-\varepsilon)}{D_p \varepsilon^3} \tag{8}$$

$$f_k = 150 \frac{1-\varepsilon}{\mathrm{Re}_p} + 1.75 \tag{9}$$

$$Re_p = \frac{D_p \rho u}{\mu}(1-\varepsilon) \tag{10}$$

where D_p is the equivalent diameter of the metallic foam, expressed as $D_p = 6/S_v$. The Reynolds number (Re_p) is based on the equivalent particle diameter. S_v is the solid surface area per unit volume. In order to consider the effect of the equivalent diameter of the metallic foam, Ref. [23] proposed the following equation:

$$S_v = \frac{4\varepsilon}{d_m(1-\varepsilon)} \tag{11}$$

where d_m is the average pore diameter of the metallic foam. Recently Liu et al. [24] modified Eq. 11 to reach the following friction factor for the metallic foams:

$$f_k = 22 \frac{1-\varepsilon}{Re_p} + 0.22 \tag{12}$$

We measured the friction factors for the copper foams. Figure 5a shows the comparison between the measured

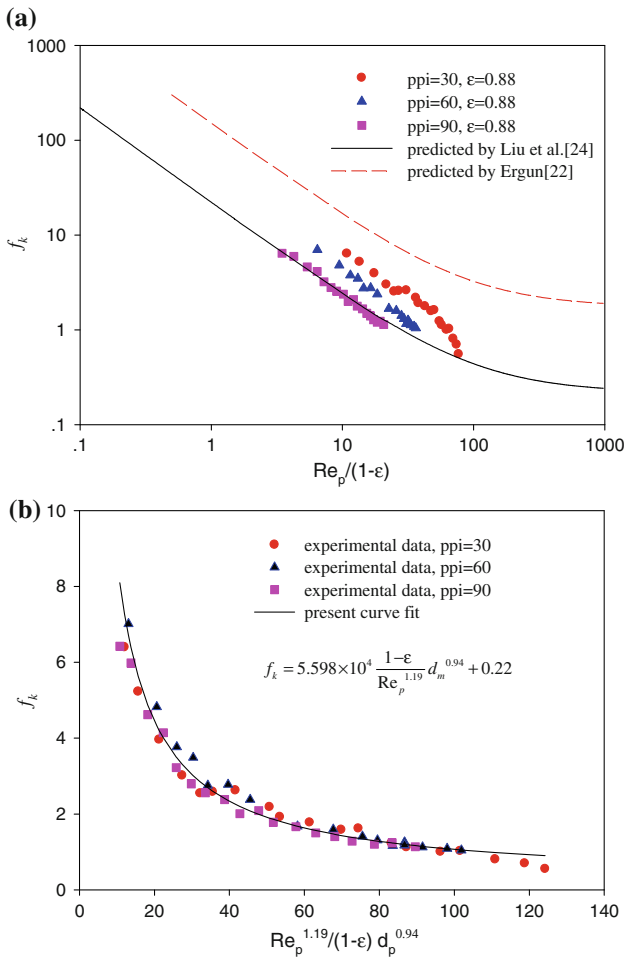

Fig. 5 Friction factors for the single-phase liquid flow in a copper foam channel

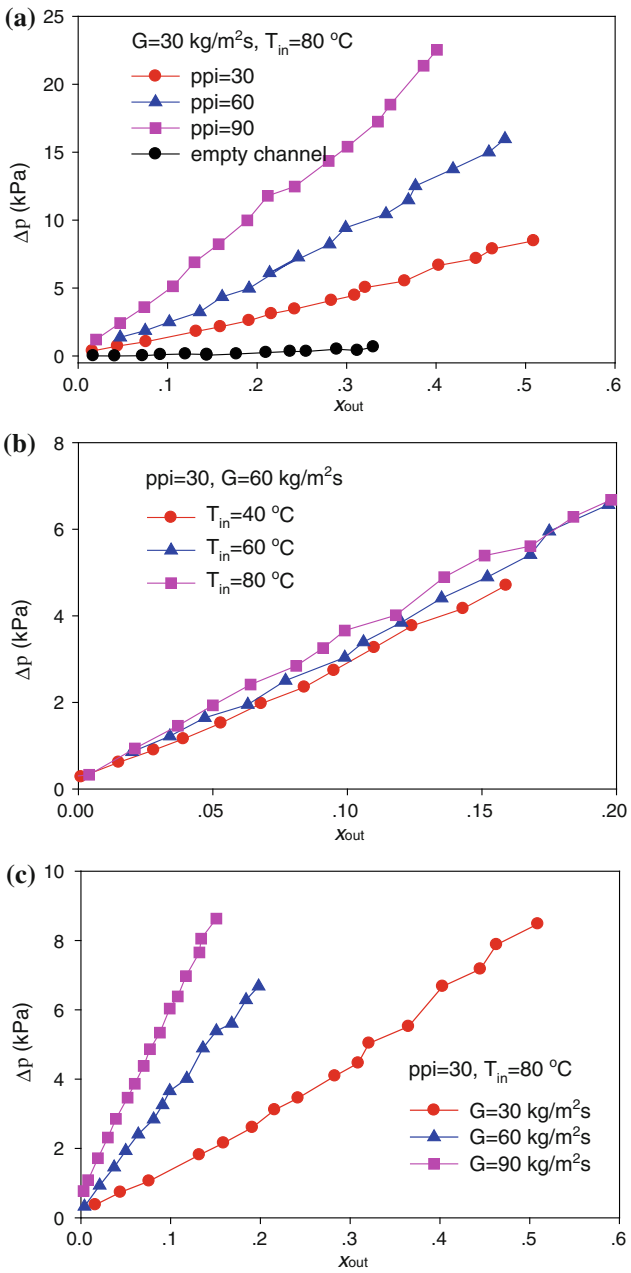

Fig. 6 The total pressure drop across the rectangular channel filled with copper foam

friction factors and the correlations given by refs. [22, 24]. In the laminar flow region at low flow velocities, the friction factors are mainly influenced by the Reynolds numbers and the average pore diameters of the copper foams. The friction factors are decreased with increases in the Reynolds numbers. Most of the experimental data are between the two predictions by Ergun [22] and Liu et al. [24]. For the 90 ppi foams, the measured friction factors are consistent well with the predictions by Liu et al. [24]. Deviations of the present measured friction factors (by Eq. 7) from the predictions by refs. [22, 24] become large with decreases in the ppi values. In order to further consider the effect of ppi values on the friction factors, the following equation is obtained based on the present experimental data:

$$f_k = 5.598 \times 10^4 \frac{1-\varepsilon}{Re_p^{1.19}} d_m^{0.94} + 0.22. \quad (13)$$

Note that the unit of d_m in Eq. 13 is m. Figure 5b shows the predictions by the present curve fit and the measured friction factors. Good agreement was achieved for all the three ppi values used in this study.

In the present study, the maximum pressure drop for the boiling heat transfer can reach 35 kPa in 90 ppi foams. The pressure drop will be much larger in the turbulent flow region. Thus we only performed the experiments in the laminar flow region. Future study will focus on the turbulent flow. It is noted that Eq. 13 is only suitable for the laminar flow region (Table 2).

For the pressure drop analysis, one must consider the entrance effect, reflecting the hydraulic boundary layer development in confined channels. Wua et al. [25] identified that the entrance length for the hydraulic boundary layer development is about a couple of times of characteristic cell size if Reynolds number is smaller than 300. Baril et al. [26] stated that when the flow is beyond a critical length about 50 times of the pore size, the entrance effect on pressure drops can be neglected. In the present study, the channel length of 52 mm is significantly larger than 2–50 pore sizes of copper foams, thus the entrance effect can be neglected.

Table 3 Two-phase pressure-drop correlations

Correlation (or model)	Reference	Frictional component, $\Delta p_{tp,f}$	Acceleration component, Δp_a	MAE (%)
1	Homogeneous model	$\Delta p_{tp,f} = L_{tp}\left(\frac{dp}{dz}\right)_l\left[1+\frac{x_{out}}{2}\left(\frac{v_{lg}}{v_l}\right)\right]$	$\Delta p_a = G^2 v_l x_{out}$	322.9%
2	Lockhart-martinelli [28]	$\Delta p_{tp,f} = \frac{L_{tp}}{x_{out}}\int_0^{x_{out}}\left(\frac{dp}{dz}\right)_l \phi_f^2 dx$	$\Delta p_a = G^2 v_l\left[\frac{x_{out}^2}{\alpha_{out}}\left(\frac{v_g}{v_l}\right)+\frac{(1-x_{out})^2}{1-\alpha_{out}}-1\right]$	
		$\phi_f^2 = 1+\frac{C}{X_{vv}}+\frac{1}{X_{vv}^2}$, C = 5	$\alpha = 1-\frac{1}{\sqrt{1+\frac{20}{x_{out}}+\frac{1}{x_{out}^2}}}$	25.8%
		$X_{vv} = \left(\frac{\mu_l}{\mu_g}\right)^{0.5}\left(\frac{1-x}{x}\right)^{0.5}\left(\frac{v_l}{v_g}\right)^{0.5}$		
3	Mishima and Hibiki [29]	$\Delta p_{tp,f} = \frac{L_{tp}}{x_{out}}\int_0^{x_{out}}\left(\frac{dp}{dz}\right)_l \phi_f^2 dx,\ \phi_f^2 = 1+\frac{C}{X_{vv}}+\frac{1}{X_{vv}^2}$	$\Delta p_a = G^2 v_l\left[\frac{x_{out}^2}{\alpha_{out}}\left(\frac{v_g}{v_l}\right)+\frac{(1-x_{out})^2}{1-\alpha_{out}}-1\right]$	
		$C = 21[1-\exp(-0.319\times 10^3 d_h)]$	$\alpha = \frac{1}{1+\left(\frac{1-x_{out}}{x_{out}}\right)\left(\frac{v_l}{v_g}\right)^{2/3}}$	31.9%
		$X_{vv} = \left(\frac{\mu_l}{\mu_g}\right)^{0.5}\left(\frac{1-x}{x}\right)^{0.5}\left(\frac{v_l}{v_g}\right)^{0.5}$		
4	Qu and Mudawar [30]	$\Delta p_{tp,f} = \frac{L_{tp}}{x_{out}}\int_0^{x_{out}}\left(\frac{dp}{dz}\right)_l \phi_f^2 dx$	$\Delta p_a = G^2 v_l\left[\frac{x_{out}^2}{\alpha_{out}}\left(\frac{v_g}{v_l}\right)+\frac{(1-x_{out})^2}{1-\alpha_{out}}-1\right]$	
		$\phi_f^2 = 1+\frac{C}{X_{vv}}+\frac{1}{X_{vv}^2}$	$\alpha = \frac{1}{1+\left(\frac{1-x_{out}}{x_{out}}\right)\left(\frac{v_l}{v_g}\right)^{2/3}}$	41.8%
		$C = 21[1-\exp(-0.319\times 10^3 d_h)](0.00418G+0.0613)$		
		$X_{vv} = \left(\frac{\mu_l}{\mu_g}\right)^{0.5}\left(\frac{1-x}{x}\right)^{0.5}\left(\frac{v_l}{v_g}\right)^{0.5}$		
5	Ji and Xu (present study)	$\Delta p_{tp,f} = \frac{L_{tp}}{x_{out}}\int_0^{x_{out}}\left(\frac{dp}{dz}\right)_l \phi_f^2 dx$	$\Delta p_a = G^2 v_l\left[\frac{x_{out}^2}{\alpha_{out}}\left(\frac{v_g}{v_l}\right)+\frac{(1-x_{out})^2}{1-\alpha_{out}}-1\right]$	
		$\phi_f^2 = 1+\frac{C}{X_{vv}}+\frac{1}{X_{vv}^2}$	$\alpha = \frac{1}{1+\left(\frac{1-x_{out}}{x_{out}}\right)\left(\frac{v_l}{v_g}\right)^{2/3}}$	7.18%
		$C = 0.025G^{1.801}e^{8.021x}d_m^{0.455}$		
		$X_{vv} = \left(\frac{\mu_l}{\mu_g}\right)^{0.5}\left(\frac{1-x}{x}\right)^{0.5}\left(\frac{v_l}{v_g}\right)^{0.5}$		

6.2 The two-phase multiplier

It is noted that various factors influence the two-phase pressure drops in metallic foams. Figure 6 shows the total pressure drop across the test section versus the outlet vapor mass qualities at different running parameters: ppi values, inlet liquid temperatures, and mass fluxes. Figure 6a identifies the fact that the pressure drop in the empty channel without copper foam inset is significantly lower than those in the copper foam channel. Figure 6b shows that the pressure drops are slightly larger at higher inlet liquid temperatures. But the differences of the pressure drops among different inlet liquid temperatures are not large. This is because the two-phase pressure drop contributes the major part of the total pressure drop. Figure 6c shows that the total pressure drops are quite sensitive to the mass fluxes. The larger the mass flux, the higher the pressure drop is. All the three subfigures in Fig. 6 shows that the total pressure drop is increased with increases in the outlet vapor mass qualities, according to a quasi-linear manner.

The total pressure drop (Δp) consists of the pressure drops in the single-phase liquid flow section (Δp_{sp}) and the two-phase flow section (Δp_{tp}). Besides, the two-phase pressure drop also includes three components: the two-phase friction pressure drop ($\Delta p_{tp,f}$), the acceleration pressure drop (Δp_a), and the gravitational pressure drop (Δp_g). We note that Δp_g should be zero with the test section horizontally positioned, such as encountered in the present study. In a real application of the heat transfer devices, the pressure drop also includes the component with the fluid flowing across an enlarged or contracted geometry, i.e., Δp_c. Thus the two-phase friction pressure drop is calculated as

$$\Delta p_{tp,f} = \Delta p - \Delta p_{sp} - \Delta p_a - \Delta p_c. \quad (14)$$

Various two-phase friction pressure drop models have been developed in the literature, including the homogeneous model and separated flow model. The two-phase friction pressure drop in metallic foams is less reported previously. Even though metallic foam belongs to the family of porous media, metal foam has distinct features compared with conventional porous media. Metal foam has quasi-ordered cell structure and large porosity such as 0.9 used in this study. Bonnet et al. [15] used the homogeneous model, Lockart–Martinelli model and separated flow model to compute the two-phase pressure drops in metallic foams, large differences are found between the model predictions and the experimental results for metallic foams. Hetsroni et al. [27] stated that most of correlations on packed beds

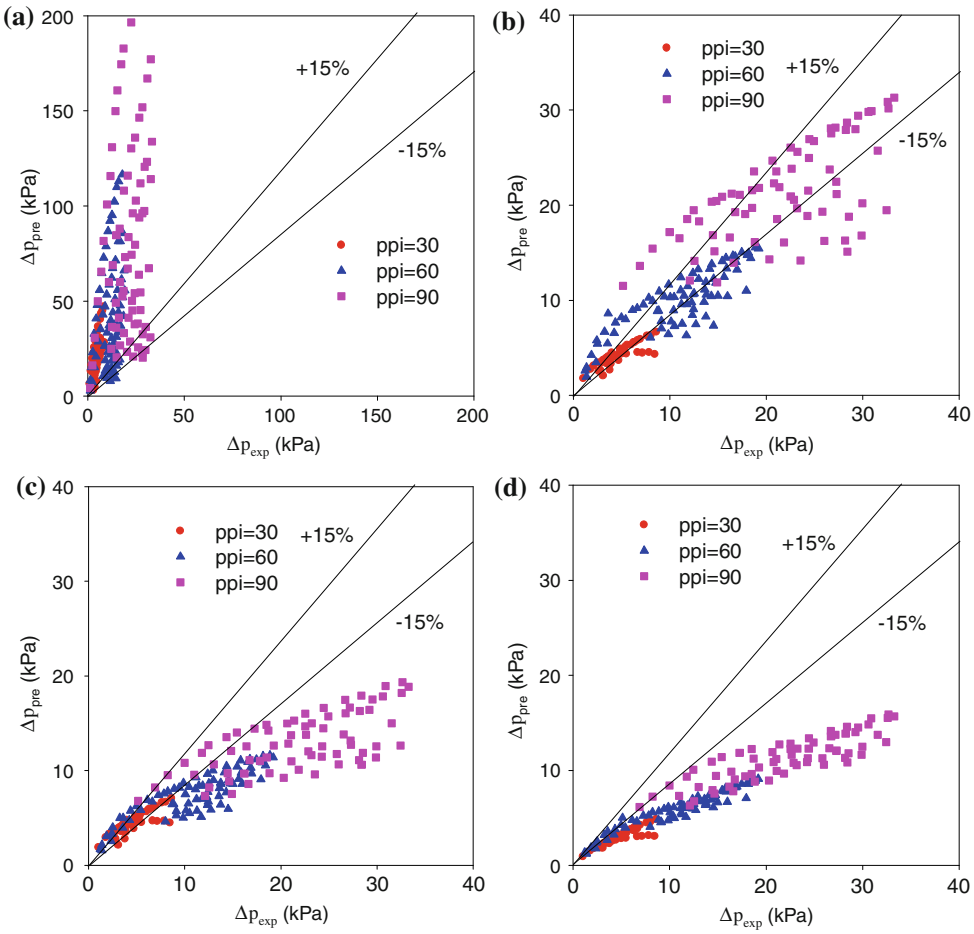

Fig. 7 Comparisons of the experimental data with the correlations in the references. **a** homogeneous model, **b** Lockhart-Martinelli correlation, **c** Mishima and Hibiki correlation, **d** Qu and Mudawar correlation

and granular porous media are not suitable for metallic foams. Here we use the homogeneous model, the Lockhart-Martinelli correlation [28], the Mishima and Hibiki correlation [29], and the Qu and Mudawar correlation [30] to calculate the two-phase friction pressure drops and compare these results with the present experimental data. These models or correlations are listed in Table 3. The relative error is calculated as (see Table 3).

$$\mathrm{MAE}(\%) = \frac{1}{\mathrm{M}}\sum \frac{\left|\Delta p_{pre} - \Delta p_{\exp}\right|}{\Delta p_{\exp}} \times 100\% \tag{15}$$

where M is the number of data points, Δp_{pre} and $\Delta p_{\exp}$ are the calculated and measured pressure drops. Figure 7a shows that the calculated pressure drops by the homogeneous flow model are significantly larger than the experimental data.

Now we discuss the pressure drop computations by the separated flow models. Usually the Martinelli model is used to evaluate the acceleration pressure drop. The axial vapor mass qualities are assumed to be linearly distributed along the flow direction. Thus the acceleration pressure drop in the separated flow model is expressed as

$$\Delta p_{tp,a} = G^2 v_l \left[\frac{x_{out}^2}{\alpha_{out}}\left(\frac{v_g}{v_l}\right) + \frac{(1-x_{out})^2}{1-\alpha_{out}} - 1\right] \tag{16}$$

where v is the specific volume, x is the vapor mass quality, g represents the vapor phase and l represents the liquid phase, respectively. α_{out} is the outlet void fraction, having the following expression:

$$\alpha_{out} = \frac{1}{1 + \left(\frac{1-x_{out}}{x_{out}}\right)\left(\frac{v_l}{v_g}\right)^{2/3}} \tag{17}$$

In order to calculate the two-phase friction pressure gradient, we introduce the Lockhart-Martinelli parameter X_{vv}. The two-phase multiplier for the liquid phase ϕ_f^2 is the ratio of the two-phase friction pressure gradient to that which would exist if the liquid phase were to be flowing alone in the pipe and is written as

$$\phi_f^2 = \left(\frac{dp}{dz}\right)_{tp} \Big/ \left(\frac{dp}{dz}\right)_l = 1 + \frac{C}{X_{vv}} + \frac{1}{X_{vv}^2}. \tag{18}$$

The Lockhart-Martinelli parameter X_{vv} is expressed as

$$X_{vv} = \left[\left(\frac{dp}{dz}\right)_l \Big/ \left(\frac{dp}{dz}\right)_g\right]^{1/2} = \left(\frac{\mu_l}{\mu_g}\right)^{0.5}\left(\frac{1-x}{x}\right)^{0.5}\left(\frac{v_l}{v_g}\right)^{0.5}. \tag{19}$$

where $\left(\frac{dp}{dz}\right)_l$ and $\left(\frac{dp}{dz}\right)_g$ represent the pressure gradients assuming that the liquid phase and vapor phase flowing in channels alone, respectively. Chisholm [31] recommended the C values in Eq. 18. C equals to 5 for the laminar flow. The two-phase friction pressure drop is

$$\Delta p_{tp,f} = \frac{L_{tp}}{x_{out}}\int_l^{x_{out}} \left(\frac{dp}{dz}\right)_l \phi_f^2 dx = \frac{L_{tp}}{x_{out}}\int_0^{x_{out}} \frac{f_k G^2 (1-x)^2 v_l (1-\varepsilon)}{D_p \varepsilon^3}\phi_f^2 dx. \tag{20}$$

Figure 7b shows the comparison between the Lockhart-Martinelli predictions and the measured two-phase pressure drops. The result is not satisfactory and the average relative error reaches 25.8%. We note that the surface tension force effect is increased by decreasing the channel size. Many investigators consider the channel hydraulic diameter effect. Mishima and Hibiki [29] modified the C value to have the following equation.

$$C = 21\left[1 - \exp\left(-0.319 \times 10^3 d_h\right)\right] \tag{21}$$

where d_h is the channel hydraulic diameter, the unit is m. However, modification of the C parameter did not significantly improve the accuracy of the two-phase friction

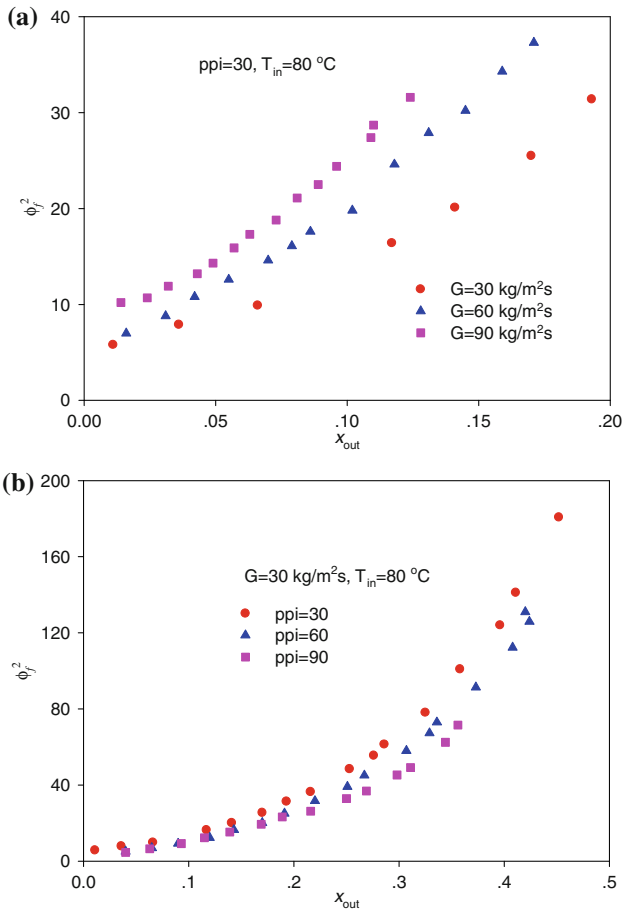

Fig. 8 The two-phase pressure gradient multiplier versus the outlet vapor mass qualities

pressure drops. Figure 7c illustrates that the predicted two-phase friction pressure drops by the Mishima and Hibiki [29] model are smaller than the measured values.

Qu and Mudawar [30] noted that considering the pore diameter of the metallic foam alone in the C parameter is not enough to improve the accuracy of the pressure drop computations. The two-phase friction pressure drop shall consider the effects of mass fluxes, channel dimensions, and flow patterns etc. Thus the following correlation for the C parameter is recommended by Qu and Mudawar [30].

$$C = 21[1 - \exp(-0.319 \times 10^3 d_h)](0.00418G + 0.0613). \quad (22)$$

When the predicted pressure drops are compared with the present experimental data, it is found that large deviations exist (see Fig. 7d). Thus new two-phase friction pressure drop correlations should be developed.

Let us re-evaluate the effect of outlet vapor mass qualities on the two-phase friction pressure drop first. Figure 8 shows that the two-phase multiplier is increased with increases in the outlet vapor mass qualities. At the same outlet vapor mass quality, the higher the mass fluxes, the larger the multiplier is (see Fig. 8a). Besides, the multiplier is larger for smaller ppi values when the outlet vapor mass quality is fixed (see Fig. 8b).

Figure 9 demonstrates the two-phase multiplier versus the Martinelli parameter X_{vv}. Generally ϕ_f^2 is decreased with increases in X_{vv}. But ϕ_f^2 approaches a constant if X_{vv} is continuously increased. For example, ϕ_f^2 is about 10 if X_{vv} is larger than 0.8 (see Fig. 9a). It is also seen from Fig. 9a, b that ϕ_f^2 is larger for larger mass fluxes at the same X_{vv}. Figure 9c gave the further evidence that ϕ_f^2 is insensitive to the inlet liquid temperatures. It is found from Fig. 9d that ϕ_f^2 is decreased with increases in the pore densities. Under the condition that the pore diameters are decreased by increasing the pore densities, the two-phase mixture approaches to be distributed uniformly in metallic foams, causing the decreased possibility of the stratification flow in the channel. In order to consider the effects of the mass fluxes, vapor mass qualities, and the average pore diameter of the metallic foams, the following correlation for the C parameter is recommended:

$$C = 0.025G^{1.801}e^{8.021x}d_m^{0.455}. \quad (23)$$

Combining Eqs. 18, 20 and 23, we can calculate the two-phase friction pressure drops in metallic foams with high porosities. Figure 10 shows the total pressure drops against the heat fluxes. The data points are the pressure

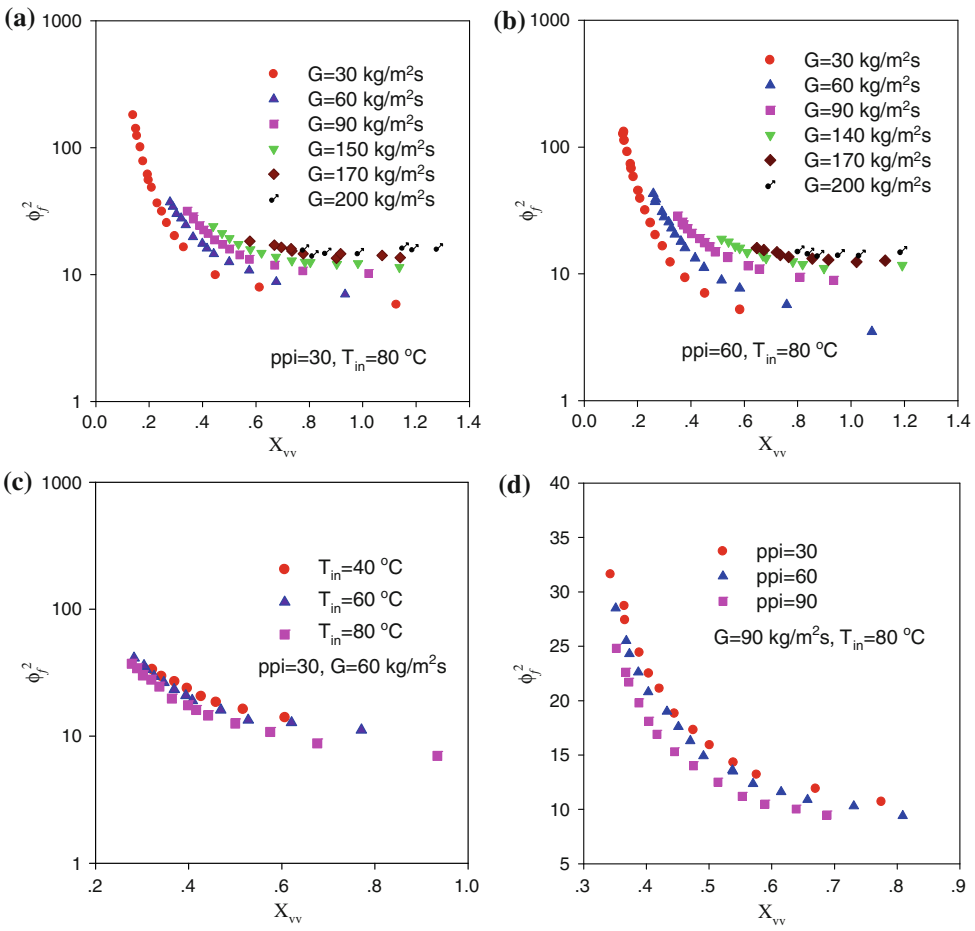

Fig. 9 The two-phase multiplier versus the Martinelli parameter

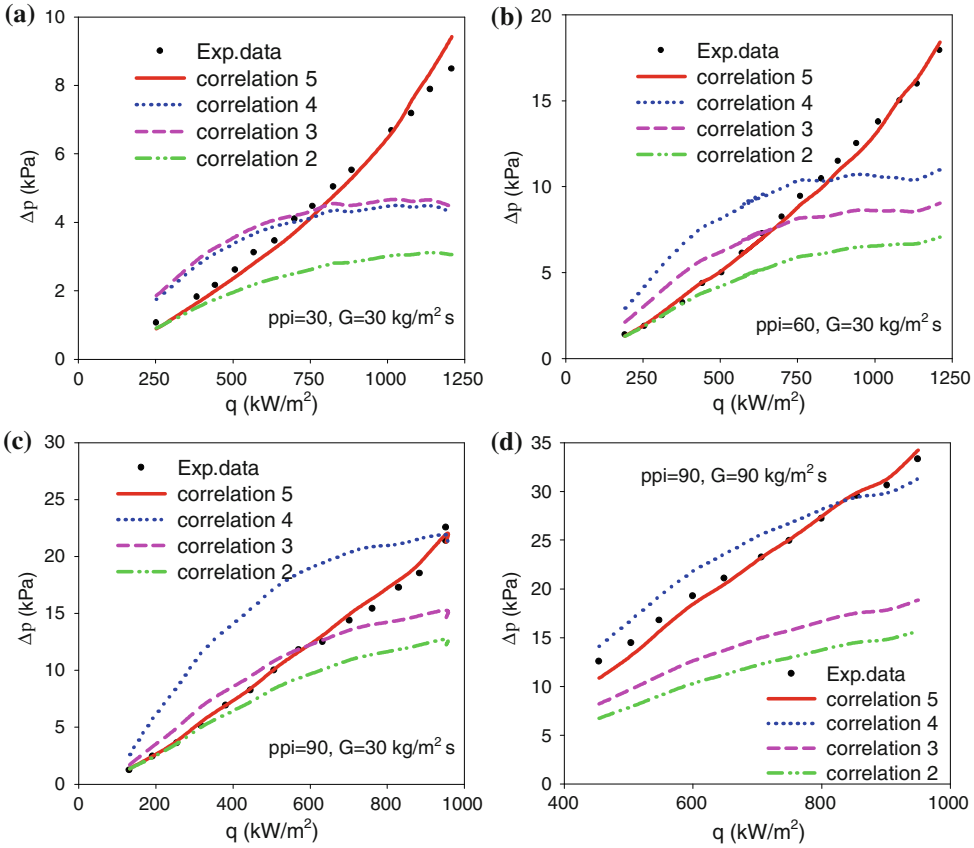

Fig. 10 Comparisons of the experimental data with various correlations (*correlation 2*: Lockhart-martinelli, *correlation 3*: Mishima and Hibiki, *correlation 4*: Qu and Mudawar, *correlation 5*: present correlation)

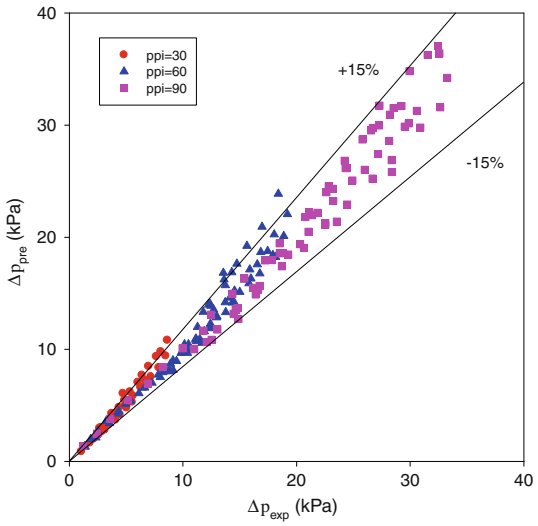

Fig. 11 Comparisons of the present measured pressure drop and the present correlations

drops measured by the pressure drop transducer. The calculated total pressure drops consist of several components which are described above, among which the two-phase friction pressure drop is evaluated based on Eqs. 18, 20 and 23. It is seen that the pressure drop predictions match the experimental data very well. Other models or correlations such as the Qu and Mudawar correlation [30], the Mishima and Hibiki correlation [29], and the Lockhart-Martinelli correlation [28] can not predict the pressure drops. Deviations of these model predictions and the measured values are large. Figure 11 shows that most of the predicted pressure drops by Eqs.18, 20 and 23 deviate from the measured values by less than 15%.

It is noted that metallic foam has network structure with foam ligaments connected each other. Heating causes bubble formation within pores and the applied pressure drop pushes bubbles to the channel downstream. Bubbles are penetrated by the foam ligament, causing large bubble deformation. An increased pressure drop shall be provided to overcome the large shear stress at the vapor–liquid interface during the bubble deformation and breakup process when the bubbles are being penetrated by the foam ligaments. The higher the heat flux, the larger number of generated bubbles is, yielding higher pressure drop. This is the reason why the pressure drops have a parabolic increase with heat fluxes, as shown in Fig. 10.

7 Conclusions

Experimental studies with the single-phase liquid flow and the boiling two-phase flow flowing in a rectangular channel filled with copper foams were studied. The following conclusions can be reached:

- The friction factors for the single-phase liquid flow are mainly dependent on the Reynolds number and the average pore diameters of the metallic foams. The friction factors are decreased with increases in the Reynolds numbers, and will approach 0.22 with high Reynolds numbers in the laminar flow region.
- Pressure drops in metallic foams are significantly larger than those in empty channels. The two-phase pressure drops are increased with increases in the outlet vapor mass qualities, mass fluxes, and ppi values.
- The two-phase multipliers are increased with increases in the outlet vapor mass qualities and mass fluxes. They are decreased with increases in the Martinelli parameter and will attain a constant value. The constant value depends on the mass fluxes. The larger the mass flux, the larger the constant value is.
- The homogeneous model, Lockhart-Martinelli model [28], Mishima and Hibiki model [29], and Qu and Mudawar model [30] can not predict the two-phase pressure drops for metallic foams. A new correlation was recommended for the C parameter, considering effects of the mass fluxes, vapor mass qualities, and the average pore diameters of the metallic foams.

Acknowledgments This paper is supported by the National Natural Science Foundation of China (U1034004 and 50825603), the Basic Research Program (973 program) with the contract number of 2011CB710703, and the Fundamental Research Funds for the Central Universities.

References

1. Lage J, Anthoe B (2000) Darcy's experiments and the deviation to nonlinear flow regime. J Fluids Eng 122:619–625
2. Dullien FAL (1979) Fluid transport and pore structure. Academic Press, New York
3. Ingham DB, Pop I (eds) (1998) Transport phenomenon in porous media. Pergamon Press, Danvers
4. Chen ZQ, Cheng P, Zhao TS (2000) An experimental study of two phase flow and boiling heat transfer in bi-dispersed porous channels. Int Commun Heat Mass Transf 27(3):293–302
5. Antohe BV, Lage JL, Price DC, Weber RM (1997) Experimental determination of permeability and inertia coefficients of mechanically compressed aluminum porous matrices. J Fluids Eng 119:404–412
6. Lage JL, Antohe BV, Nield DA (1997) Two types of nonlinear pressure-drop versus flow-rate relation observed for saturated porous media. J Fluids Eng 119:700–706
7. Bastwros AF (1998) Effectiveness of open cell metallic foams for high power electronic cooling. Anaheim: symposium on the thermal management of electronics
8. Bastawros AF, Evans AG, Stone HA (1998) Evaluation of cellular metal heat transfer media. Report MECH 325. Division of Engineering and Applied Sciences, Harvard University, Cambridge
9. Kim SY, Paek JW, Kang BH (2000) Flow and heat transfer correlations for porous fin in a plate-fin heat exchanger. J Heat Transf 122:572–578
10. Crosnier S, Riva R, Bador B, Blet V (2003) Modelling of gas flow through metallic foams presented. Alpexpo-Alpes Congrés, Grenobel, France: 1st European Hydrogen Energy Conference
11. Khayargoli P, Loya V, Lefebvre LP, Medraj M (2004) The impact of microstructure on the permeability of metal foams. In: Proceedings of CSME Forum 2004, pp 220–228
12. Dukhan N, Picón-Feliciano R, lvarez-Hernández R (2006) Air flow through compressed and uncompressed aluminum foam: measurements and correlations. J Fluids Eng 128:1004–1012
13. Medraj M, Baril E, Loya V, Lefebvre LP (2007) The effect of microstructure on the permeability of metallic foams. J Mater Sci 42(12):4372–4383
14. Salas KI, Waas AM (2007) Convective heat transfer in open cell metal foams. J of Heat Transf 129(9):1217–1229
15. Bonnet JP, Topin F, Tadrist L (2008) Experimental study of two phase flow through open-celled metallic foam. In: Proceedings of the fifth international conference on porous metals and metal foaming technology, Montreal, pp 467–470
16. Gerbaux O, Vercueil T, Memponteil A, Bador B (2009) Experimental characterization of single and two-phase flow through nickel foams. Chem Eng Sci 64:4186–4195
17. Zhao CY, Lu W, Tassou SA (2009) Flow boiling heat transfer in horizontal metal-foam tubes. J Heat Transf ASME 131:121002
18. Gibson LJ, Ashy MD (1999) Cellular solid, 2nd edn. Cambridge University Press, Cambridge
19. Venkataraman S, Sankar BV (2001) Analysis of sandwich beams with functionally graded core. In: Proceedings of the 42nd AIAA structures. Structural dynamics and materials conference, Seattle, Washington
20. Thompson W (1887) On the division of space with minimum partitional area. Philos Mag 24:503–514
21. Beckermann C, Viskanta R (1936) Forced convection boundary layer flow and heat transfer along a flat plate embedded in a porous medium. Int J Heat Mass Transf 30:1547–1551
22. Ergun S (1952) Fluid flow through packed columns. Chem Eng Prog 48:89–94
23. Richardson JT, Peng Y, Remue D (2000) Properties of ceramic foam catalyst supports: pressure drop. Appl Catal A Gen 204:19–32
24. Liu JF, Wu WT, Chiu WC, Hsieh WH (2006) Measurement and correlation of friction characteristic of flow through foam matrixes. Exp Thermal Fluid Sci 30:329–336
25. Wua Z, Caliot C, Bai F, Flamant G, Wang ZFG, Zhang JS, Tian C (2010) Experimental and numerical studies of the pressure drop in ceramic foams for volumetric solar receiver applications. Appl Energy 87:504–513
26. Baril E, Mostafid A, Lefebvre LP, Medraj M (2008) Experimental Demonstration of Entrance/Exit Effects on the Permeability Measurements of Porous Materials. Advanced Engineering Materials 10(9):889–894
27. Hetsroni G, Gurevich M, Rozenblit R (2005) Metal foam heat sink for transmission window. International Journal of Heat and Mass Transfer 48:3793–3803
28. Lockhart RW, Martinelli RC (1949) Proposed correlation of data for isothermal two-phase, two-component flow in pipes. Chem Eng Prog 45:39–48
29. Mishima K, Hibiki T (1996) Some characteristics of air–water two-phase flow in small diameter vertical tubes. Int J Multiphase Flow 22:703–712
30. Qu W, Mudawar I (2003) Measurement and prediction of pressure drop in two-phase micro-channel heat sinks. International Journal of Heat and Mass Transfer 46:2737–2753
31. Chisholm D (1968) The influence of mass velocity on friction pressure gradients during steam-water flow, Paper 35 presented at 1968 Thermodynamics and Fluid Mechanics Convention I. Mech Engrs Bristol, March 1968